THE JOURNAL OF BIOLOGICAL CHEMISTRY VOL. 287, NO. 19, pp. 16047–16057, May 4, 2012
© 2012 by The American Society for Biochemistry and Molecular Biology, Inc. Published in the U.S.A.

Dual Color Photoactivation Localization Microscopy of Cardiomyopathy-associated Desmin Mutants*[S]

Received for publication, October 14, 2011, and in revised form, February 27, 2012 Published, JBC Papers in Press, March 8, 2012, DOI 10.1074/jbc.M111.313841

Andreas Brodehl[‡], Per Niklas Hedde[§], Mareike Dieding[¶], Azra Fatima[‖], Volker Walhorn[¶], Susan Gayda[§], Tomo Šarić[‖], Bärbel Klauke[‡], Jan Gummert[**], Dario Anselmetti[¶], Mike Heilemann[‡‡1], Gerd Ulrich Nienhaus[§ §§2], and Hendrik Milting[‡3]

*From the [‡]E. & H. Klessmann Institute for Cardiovascular Research & Development and the **Clinic of Cardio-Thoracic Surgery, Heart and Diabetes Center NRW, Ruhr-University Bochum, 32545 Bad Oeynhausen, Germany, the [§]Institute of Applied Physics and Center for Functional Nanostructures, Karlsruhe Institute of Technology, 76128 Karlsruhe, Germany, the [¶]Experimental Biophysics and Applied Nanoscience, Faculty of Physics and Bielefeld Institute for Biophysics and Nanoscience (BINAS), Bielefeld University, 33615 Bielefeld, Germany, the [‖]Institute for Neurophysiology, Medical Center, University of Cologne, 50931 Cologne, Germany, the [‡‡]Department of Biotechnology & Biophysics, Julius-Maximilians-University Würzburg, 97074 Würzburg, Germany, and the [§§]Department of Physics, University of Illinois at Urbana-Champaign, Urbana, Illinois 61801*

Background: Heterozygous *DES* mutations affect filament formation leading to skeletal and cardiomyopathies.
Results: Our results reveal different extent of filament formation defects by various desmin mutants under heterozygous conditions.
Conclusion: Analysis of interaction and co-localization of mutant and wild-type desmin proves the co-existence of heterogeneous filaments in living cells.
Significance: These results might be of relevance for the understanding of filament formation defects.

Mutations in the *DES* gene coding for the intermediate filament protein desmin may cause skeletal and cardiac myopathies, which are frequently characterized by cytoplasmic aggregates of desmin and associated proteins at the cellular level. By atomic force microscopy, we demonstrated filament formation defects of desmin mutants, associated with arrhythmogenic right ventricular cardiomyopathy. To understand the pathogenesis of this disease, it is essential to analyze desmin filament structures under conditions in which both healthy and mutant desmin are expressed at equimolar levels mimicking an *in vivo* situation. Here, we applied dual color photoactivation localization microscopy using photoactivatable fluorescent proteins genetically fused to desmin and characterized the heterozygous status in living cells lacking endogenous desmin. In addition, we applied fluorescence resonance energy transfer to unravel short distance structural patterns of desmin mutants in filaments. For the first time, we present consistent high resolution data on the structural effects of five heterozygous desmin mutations on filament formation *in vitro* and in living cells. Our results may contribute to the molecular understanding of the pathological filament formation defects of heterozygous *DES* mutations in cardiomyopathies.

Desmin is a 53-kDa highly conserved muscle-specific intermediate filament (IF)[4] protein. Missense mutations and small deletions in the desmin (*DES*) gene have been linked to skeletal and cardiac myopathies (1–4). In many cases, these mutations result in a loss of the filamentous network caused by abnormal aggregation of desmin and desmin-associated proteins (5). For clinical diagnosis of desmin-related myopathy or cardiomyopathy, histological examination of aggregate formation is often used. In patients suffering from arrhythmogenic right ventricular cardiomyopathy (ARVC), several groups recently identified different mutations in the *DES* gene (6–9). ARVC is a heritable cardiomyopathy, which is pathologically characterized by predominant dilatation of the right ventricle and arrhythmias often leading to heart failure or even sudden cardiac death. However, little is known about the molecular and cellular pathomechanisms of ARVC-associated desmin mutations. In healthy cardiomyocytes, desmin forms a three-dimensional scaffold around myofibrillar z-bands and connects desmosomes as well as costamers to the contractile apparatus, thus providing cellular stability (2, 10, 11). Like other IF proteins, desmin consists of a central α-helical rod domain of 310 amino acids flanked by nonhelical head and tail domains. Previously, it was proposed that the rod domain is divided into four fragments (1A, 1B, 2A, and 2B) by three nonhelical linker regions (12). However, recent crystallographic studies of rod domain-localized fragments of the homologous IF protein vimentin demonstrated that coil 1 and coil 2 are *not* separated by nonhelical linker regions (13, 14). A generally accepted model for the

* This work was supported by Grant O1 GN 0824 from the German Ministry of Education and Research (BMBF) to (T. Š.).
[S] This article contains supplemental text, Table SI, and Figs. S1–S3.
[1] Supported by German Ministry of Education and Research (BMBF) Grant 0315262.
[2] Supported by the Deutsche Forschungsgemeinschaft and the state of Baden-Württemberg through the Center for Functional Nanostructures and by Deutsche Forschungsgemeinschaft Grant Ni 291/9.
[3] Supported by the Erich and Hanna Klessmann Foundation (Gütersloh, Germany) and by FoRUM Grant F649-2009 of the Ruhr-University Bochum. To whom correspondence should be addressed: E. & H. Klessmann Institute for Cardiovascular Research & Development, Heart and Diabetes Center NRW, Ruhr-University Bochum, D-32545 Bad Oeynhausen, Germany. Tel.: 49-5731-973510; Fax: 49-5731-972476; E-mail: hmilting@hdz-nrw.de.

[4] The abbreviations used are: IF, intermediate filament; ARVC, arrhythmogenic right ventricular cardiomyopathy; hiPS-CM, cardiomyocyte derived from human induced pluripotent stem cells; AFM, atomic force microscopy; PALM, photoactivation localization microscopy; eYFP, enhanced yellow fluorescent protein.

in vitro assembly process was developed by numerous investigations (see Ref. 15 for a review). Presumably, desmin assembly can be divided into three major steps. In the first step, unit-length filaments are built by lateral association of eight tetramers, each consisting of two coiled-coil dimers arranged in an anti-parallel alignment. In the second step, short filaments are formed by longitudinal annealing of unit-length filaments. In the third assembly step, these filaments are extended into wide filaments with a typical diameter of ~10–15 nm (12).

In most studies, desmin mutants were investigated in homozygously transfected cells by immunohistochemistry (4, 8, 16, 17). However, in the clinical setting, *DES* mutations are usually heterozygous and lead to autosomal dominant inheritance. Previous *in vitro* investigations are of limited value, because wild-type and mutant desmin molecules could not be differentiated. Therefore, it is currently unknown whether mutant desmin molecules disrupt filament formation of wild-type desmin or whether both forms are incorporated into the same filament when co-expressed. Furthermore, previous studies on desmin filament formation were compromised by the limited resolution of conventional far field microscopy.

In this study, we have focused on the heterozygous character of ARVC-associated *DES* mutations. First, we compared filament and aggregate formation of five ARVC-associated desmin mutations in homozygously transfected SW-13, H9c2, HL-1, and C2C12 cells and in cardiomyocytes derived from human induced pluripotent stem cells (hiPS-CMs). We further assessed filament formation of different mutants at the molecular level by atomic force microscopy (AFM) to understand which step of filament formation is impaired by the mutants. Furthermore, we investigated whether co-expression of mutant and wild-type desmin disturbs filament assembly using super-resolution dual color photoactivation localization microscopy (PALM) and FRET in combination with confocal microscopy.

EXPERIMENTAL PROCEDURES

Cell Culture, Transfection, and Fluorescence Microscopy—SW-13, H9c2, and C2C12 cells (LGC Standards, Middlesex, UK) were grown in culture dish assemblies on glass cover slides in DMEM (Invitrogen) supplemented with 10% FBS and penicillin/streptomycin (Invitrogen). HL-1 cardiomyocytes were kindly provided by W. C. Claycomb (18) and cultured in Claycomb medium (Sigma-Aldrich) supplemented with 10% FBS, penicillin/streptomycin, 2 mM L-glutamine, and 0.1 mM norepinephrine. Cardiac differentiation of hiPS cell line derived from foreskin fibroblasts, clone 1 (19), was carried out on the murine visceral endoderm-like cell line END2 in knock-out DMEM containing 1 mM L-glutamine, 1% nonessential amino acids, 0.1 mM β-mercaptoethanol, and penicillin/streptomycin as described earlier (20, 21). The co-culture was left undisturbed at 37 °C for 4 days. The first medium change was performed on day 5 and later on days 9, 12, and 15 of differentiation. Spontaneously beating areas from hiPS-CM cultures were microdissected on day 25 of differentiation and dissociated into single cells by trypsinization. Single hiPS-CM were plated on fibronectin-coated (2.5 μg/ml) dishes in Iscove's modified Dulbecco's medium supplemented with 10% FBS containing 1 mM L-glutamine, 1% nonessential amino acids, 0.1 mM β-mercaptoethanol, and penicillin/streptomycin. The cells were transfected using Lipofectamine 2000 (Invitrogen) according to the manufacturer's protocol using 800 ng of plasmid DNA for a single transfection and 400 ng of each plasmid for co-transfections. For details on the plasmids, see supplemental Table SI. The medium was replaced 8 h after transfection. 24 h later, the cells were fixed in 4% paraformaldehyde, permeabilized with 0.1% Triton X-100, and blocked with 5% FBS and then stained overnight at 4 °C with primary antibodies against sarcomeric α-actinin (Sigma-Aldrich) and later with Alexa Fluor 555 conjugated anti-mouse IgG1 secondary antibody (Molecular Probes). The nuclei were stained with Hoechst 33342. The samples were embedded in ProLong Gold antifade reagent (Invitrogen). Fluorescence images were recorded with an Eclipse TE2000-U microscope (Nikon, Tokyo, Japan) equipped with a digital sight DS-2MV CCD camera (Nikon); YFP, Cy3, and DAPI filter sets (AHF, Tübingen, Germany); and an oil immersion objective (Plan Apochromat 60×/1.40 oil; Nikon).

Immunoblotting—24 h after transfection, the cells were harvested using 200 μl of ProFound lysis buffer (Thermo Scientific, Waltham, MA) containing 1 mM proteinase inhibitor mixture (Sigma-Aldrich). After homogenization and centrifugation, the concentrations of the solubilized proteins were measured by the BCA method. Equal amounts of total lysates were separated by SDS-PAGE and electrotransferred (Trans-blot SD; Bio-Rad) to nitrocellulose membranes (Bio-Rad). After blocking for 1 h in 5% fat free milk powder in TBS, the membranes were incubated overnight at 4 °C with antibodies against desmin (200 ng/ml; R & D Systems, Minneapolis, MN) and GAPDH (20 ng/ml; Abcam, Cambridge, UK). After rigorous washing, the membranes were incubated with HRP-conjugated secondary antibodies against goat (100 ng/ml; R & D Systems) or mouse IgG (400 ng/ml; BD Pharmingen, San Diego, CA) for 1 h at room temperature followed by washing the membranes with TBST. Chemiglow (Cell Biosciences, Santa Clara, CA) was used as a substrate for HRP. Chemiluminescence signals were recorded with a CCD camera system (Cell Biosciences) and analyzed with the Alpha View FluorChem FC2 software (Cell Biosciences).

Immunostaining—SW-13 cells were transfected with desmin expression constructs without any fluorescent tag. 24 h after transfection, the cells were washed three times with PBS, fixed in 4% paraformaldehyde, permeabilized with 0.1% Triton X-100 (20 min at room temperature), blocked with 5% FBS, and then stained overnight at 4 °C with primary antibodies against desmin (R & D Systems) and later with Cy3-conjugated secondary antibody against goat IgG (Jackson ImmunoResearch, Suffolk, UK).

Desmin Expression, Purification, and Folding—Bacterial cells (*Escherichia coli* BL21Star DE3), transformed with the corresponding plasmids, were grown in LB medium at 37 °C to an $A_{600\,nm}$ of 0.5–0.8 in a shaking incubator. Protein expression was induced with isopropyl β-D-thiogalactopyranoside (1 mM). After 4 h, the bacteria were harvested by centrifugation, and inclusion bodies were prepared as previously described (8). Inclusion bodies containing recombinant desmin molecules were finally dissolved in buffer composed of 8 M urea, 10 mM Tris-HCl, 100 mM NaH_2PO_4, pH 8.0. After centrifugation (45 min at 4 °C at 45,000 *g*), the supernatants were supplied to a HiTrap DEAE-Sepharose Fast Flow column (GE Healthcare)

using a FPLC system (GE Healthcare). Desmin molecules were eluted by a linear salt gradient (0–0.35 M NaCl), and purification of recombinant desmin was analyzed by SDS-PAGE and Coomassie Blue R-250 staining. Fractions containing desmin were pooled and purified with a Ni^{2+}-NTA-Sepharose column (Qiagen). The column was washed with buffer (8 M urea, 20 mM Tris-HCl, 10 mM imidazole, pH 8.0) until the absorbance at 280 nm decreased to a constant value below 0.01. Afterward, recombinant desmin molecules were eluted with imidazole-containing buffer (8 M urea, 20 mM Tris-HCl, 300 mM imidazole, pH 6.9). Fractions containing more than 95% recombinant desmin were pooled and stored at −80 °C. Purified recombinant desmin was dialyzed against buffer (20 mM Tris-HCl, 1 mM DTT, 1 mM EDTA, 0.1 mM EGTA, and 10 mM NH_4Cl, pH 8.4) as previously described (8). Protein concentrations were determined by the BCA assay according to the manufacturer's instructions (Sigma-Aldrich) using BSA as a standard.

Atomic Force Microscopy—Filament assembly of recombinant desmin was initiated immediately after dialysis by adding an equal volume of assembly buffer (100 mM NaCl, 45 mM Tris-HCl, pH 7.0) and subsequent heating to 37 °C for 1 h (22). The assembled desmin filaments (12.5 μg/ml) were applied to freshly cleaved mica substrates (Plano, Wetzlar, Germany), rinsed with deionized water to remove unbound protein, and dried under a gentle flow of nitrogen. Topographic AFM imaging was done in ambient conditions with a Mutimode AFM and Nanoscope IIIa controller (Bruker, Santa Barbara, CA) in tapping mode using Tap300AI-G (Budget Sensors, Sofia, Bulgaria) or PPP-NCH (Nanosensors, Neuchatel, Switzerland) probes.

Photoactivation Localization Microscopy—After cell transfection, PALM images were acquired on a modified inverted microscope (Axiovert 200; Zeiss, Jena, Germany). Three diode-pumped solid state lasers supplied the laser lines 561 nm (GCL-150-561; CrystaLaser, Reno, NV), 473 nm (LSR473-200-T00; Laserlight, Berlin, Germany), and 405 nm (CLASII 405-50; Blue Sky Research, Milpitas, CA) for excitation and photoactivation of the fluorophores. All of the laser sources were combined via dichroic mirrors (AHF) and coupled into a single mode fiber (OZ Optics, Ottawa, Canada). During the experiment, laser intensities were controlled via an acousto-optic tunable filter (AOTFnC-400.650, A-A; Opto-Electronic, Orsay, France). Before and after PALM imaging, we recorded a bright field image of each cell to monitor cell viability. PALM images of single transfected cells expressing mEosFP*thermo* fusion proteins were acquired using an electron multiplying charge coupled device camera (Ixon DV887ECS-BV; Andor, Belfast, UK). A total of 10,000–20,000 frames using a camera exposure time of 50 ms were recorded for each high resolution image. Wide field excitation of the red form of mEosFP*thermo* was performed with 561-nm laser light at 0.3–0.5 kW/cm^2; green-to-red conversion was induced by 405-nm laser light at 0–0.02 kW/cm^2. Fluorescence light was filtered by a 610/75-nm bandpass (Chroma HQ 610/75; AHF) after passing the excitation dichroic mirror (z 405/473/561; AHF). PALM images of co-transfected cells expressing mEosFP*thermo* as well as mIrisGFP1 fusion proteins were recorded using a different electron multiplying charge coupled device camera (Ixon EM+ DU-860; Andor, Belfast, UK), which allowed faster imaging with an exposure time of 3 ms/frame, each of which consisted of 128 × 128 pixels. For each PALM image, 5,000–20,000 frames were recorded depending on the protein expression of the individual cells. Wide field excitation of the red form of mEosFP*thermo* was performed with 561-nm laser light at 2.5–4.5 kW/cm^2; green-to-red conversion was induced by 405-nm laser light at 0–0.2 kW/cm^2. For excitation and off switching of mIrisGFP1, 473-nm light at 2.8–3.6 kW/cm^2 was used, whereas on switching was induced by 405-nm light at 0–0.2 kW/cm^2. Fluorescence light was separated by the excitation dichroic mirror and filtered by a 610/75-nm bandpass for detection of red fluorescence and by a 535/70-nm bandpass (Chroma HQ 535/70; AHF) for detection of green fluorescence. All of the PALM images shown were analyzed by fitting a two-dimensional Gaussian distribution to the single molecule signals detected using a homemade algorithm written in Matlab (Matlab R2010b; The MathWorks, Natick, MA) (23, 24). According to the strategy of Shroff *et al.* (25), data acquisition was stopped in the red and started in the green channel when no more molecules were detectable in the red channel under photoconverting 405-nm irradiation. In this way, we ensured that all of the molecules had been photoconverted and subsequently bleached. In controls we confirmed that all mEosFP*thermo*-molecules ("green") were indeed converted to their red-emitting forms using singly transfected cells under identical experimental conditions as compared with the dual color experiments. After photo-conversion with 405-nm light, no mEosFP*thermo* molecules were detectable in the green channel (supplemental Fig. S2, *A* and *B*). For control purposes, we also checked whether mIrisGFP1 was not converted to a red emitting form. We imaged cells transfected with mIrisGFP1 with the same illumination protocol as for the dual color experiments. No mIrisGFP1 molecules were detectable in the red channel under these conditions (supplemental Fig. S2, *C* and *D*).

FRET Imaging—FRET measurements were performed on a confocal laser scanning microscope LSM710 (Zeiss) equipped with an oil immersion objective (Plan-Apochromat 63×/1.40 oil; Zeiss). In each FRET experiment, three different images were recorded. First, the donor fluorophore enhanced cyan fluorescent protein was excited at 458 nm, and the fluorescence emission was detected in the spectral range of 462–515 nm. Second, the fluorescence signal of the acceptor fluorophore eYFP was detected in the spectral range of 554–651 nm (458 nm, excitation; apparent FRET signal). Third, the acceptor fluorophore eYFP was excited at 514 nm, and the fluorescence emission was detected in the spectral range of 554–651 nm. A corrected FRET signal was obtained by correcting for leakage of the donor fluorescence emission into the acceptor detection range and for direct excitation of acceptor fluorophore (26). This correction requires two correction factors ($\alpha = 0.599 \pm 0.147$; $\beta = 0.488 \pm 0.051$) for donor leakage and direct excitation of the acceptor (26), which were determined from 10 individual transfected cells expressing only the donor or the acceptor fusion protein. Image processing was performed using the ImageJ plug-in FRET and colocalization analyzer (27).

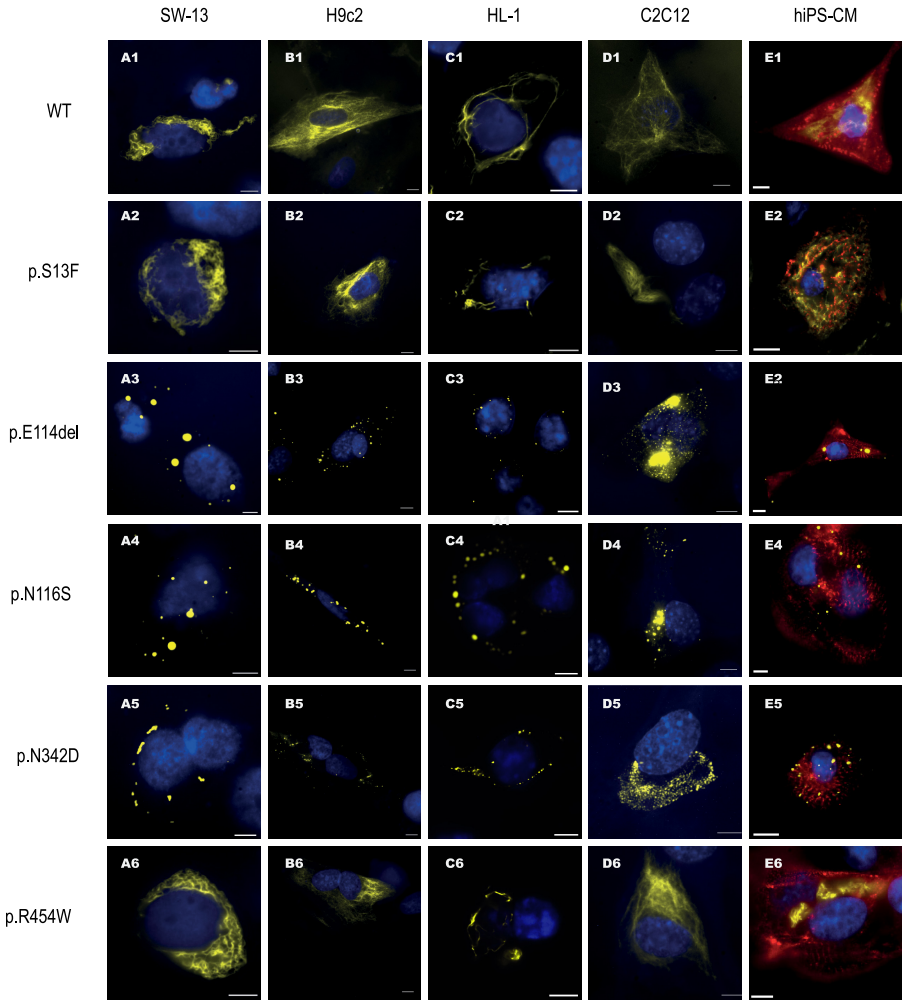

FIGURE 1. **Aggregate formation of ARVC-associated desmin mutants in transfected cells.** Representative fluorescence images of transfected SW-13, H9c2, HL-1, C2C12, and hiPS-CM expressing desmin-eYFP constructs (*yellow*) are shown. *Row 1*, wild type; *row 2*, p.S13F; *row 3*, p.N116S; *row 4*, p.E114del; *row 5*, p.N342D; *row 6*, p.R454W. The nuclei were stained with DAPI or Hoechst 33342 (*blue*), and cardiomyocytes in human iPS cell cultures were identified by staining with α-actinin and Alexa Fluor 555-conjugated secondary antibodies (*red*). The *scale bars* represent 10 μm.

RESULTS

Cytoplasmic Aggregate Formation by Desmin Mutants in Transfected Cells—To compare filament or aggregate formation of different ARVC-associated desmin mutants, we generated expression constructs of desmin wild type, p.S13F, p.E114del, p.N116S, p.N342D, and p.R454W fused at the C terminus to eYFP and analyzed filament and aggregate formation in homozygously transiently transfected SW-13, H9c2, HL-1, C2C12 cells, and hiPS-CM. Because we used tagged desmin constructs carrying fluorescent proteins at the C terminus, we and others (28) excluded an influence of the tag on filament or aggregate formation by immunolabeling (see Fig. 2*C*).

In agreement with other studies (8, 9, 29), we detected cytoplasmic aggregates with p.E114del, p.N116S, and p.N342D independent of the transfected cell type (Fig. 1, *rows 3–5*). In contrast, the mutant p.S13F and p.R454W assembled into filamentous networks (Fig. 1, *rows 2* and *6*) similar to wild-type desmin (Fig. 1, *row 1*), and the proportion of cells with aggregates reached no significant level in comparison with wild-type transfected cells (Fig. 2*A*). These results were also verified by high resolution PALM on SW-13 cells (Fig. 3). Because differences in protein expression levels between individual desmin mutants might contribute to their different aggregation propensities in cells, we compared the expression levels of the different desmin mutants with the wild-type desmin using immunoblotting (Fig. 2*B*). In all of the experiments, the expression levels of transfected desmin forms were comparable and therefore were not causative for aggregate formation (Fig. 2*B* and supplemental Fig. S3). Furthermore, we analyzed in H9c2, C2C12, and HL-1 cells the ratio of the endogenously and exogenously expressed desmin by semiquantitative immunoblotting (supplemental Fig. S3). These data indicate that 2–4% of the desmin can be accounted to the endogenous desmin in all transfected cells and is therefore negligible.

Analysis of Filament Assembly of Mutant and Wild-type Desmin by AFM—To investigate filament formation of the different desmin mutants at the molecular level, we expressed mutant and wild-type desmin in *E. coli* and investigated the structures of the purified proteins by AFM. The purity of the recombinantly expressed molecules was assessed by SDS-PAGE and Coomassie Blue staining (supplemental Fig. S1). As expected, wild-type desmin formed filaments of variable length.

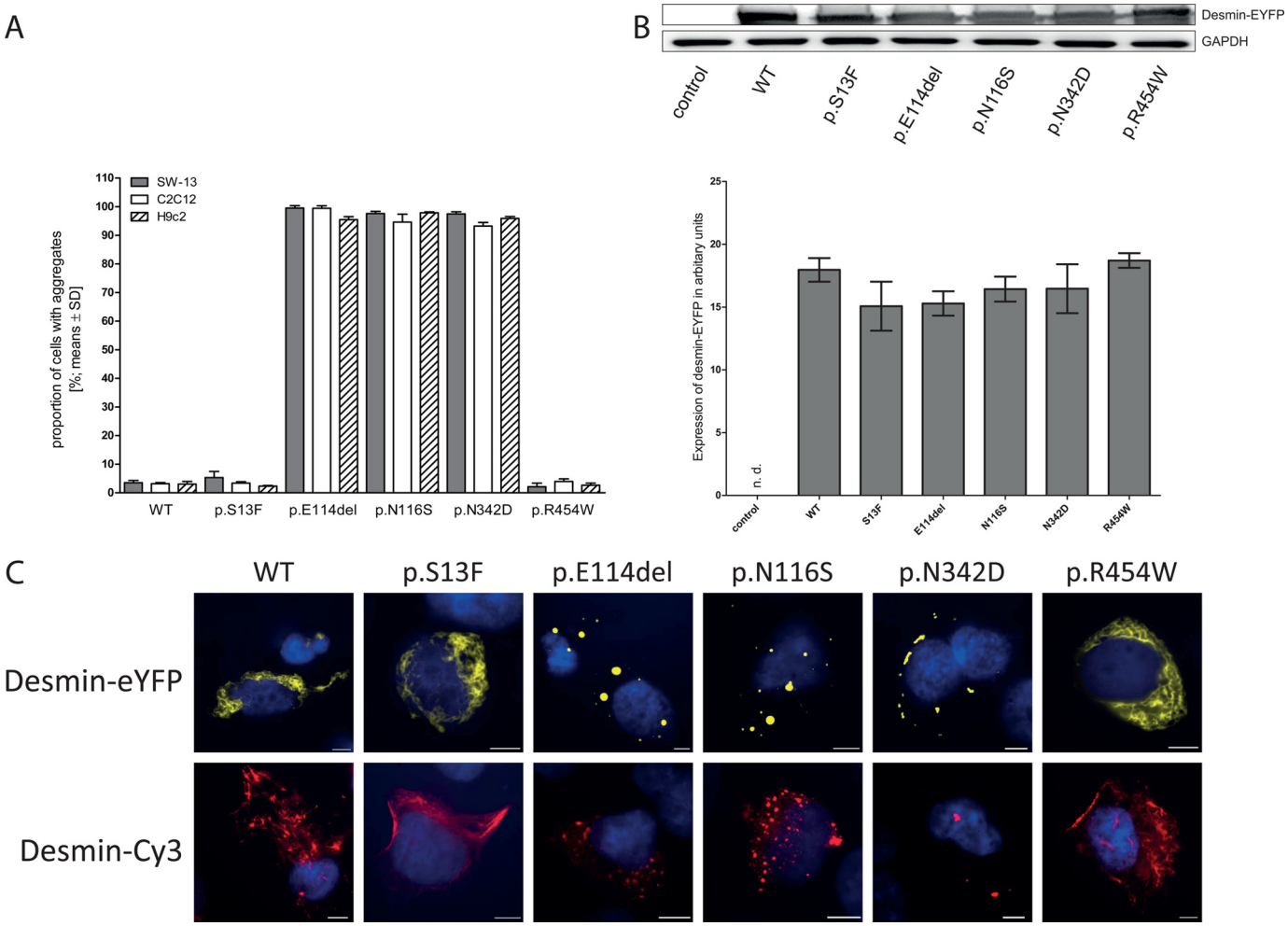

FIGURE 2. **Validation of different desmin expressing plasmids and assessment of their ability to form aggregates in control cells.** *A*, wild-type and different mutant desmins were transiently expressed in SW-13, C2C12, and H9c2 cells, and the percentage of cells containing desmin aggregates was scored. The data are given as the means ± S.D. of three independent transfection experiments. In each experiment, approximately 100 transfected cells were investigated. *B*, quantitation of desmin expression transfected SW-13 cells. The cells were transiently transfected with the specified desmin-eYFP expression constructs (80 kDa), and the cell lysates were analyzed 24 h after transfection by immunoblotting. Representative immunoblots against desmin and GAPDH (used as a housekeeping protein) are shown. The expression levels of the different desmin-eYFP expression constructs are represented as the means ± S.D. in arbitrary units of three independent experiments. *n.d.*, not detectable. *C*, tag control experiments in transfected SW-13 cells. Representative fluorescence images of desmin-eYFP (*yellow*, *row 1*) and untagged desmin stained with Cy3-conjugated secondary antibodies (*red*, *row 2*). The nuclei were stained with DAPI (*blue*). The *scale bars* represent 10 μm.

In high resolution AFM images, a coiled structure with a right-handed twist was observed (Fig. 4*A*). In contrast, all mutants with the exception of p.R454W did not assemble into regular filaments (Fig. 4, *B–E*). The mutants p.S13F and p.N116S (Figs. 2*C* and 4*B*) showed filamentous aggregates of different size. In the case of p.N342D (Fig. 4*E*), the samples were sparsely covered with irregularly shaped aggregates and small fibrils, presumably desmin tetramers or unit-length filament precursors. Interestingly, the deletion mutant p.E114del differed remarkably from the other observed filament assembly defects. This mutant did not assemble into regular filaments at all but formed fibrils that were like beads on a string (Fig. 4*D*) with a length of 114 ± 55 nm ($n = 88$), which is significantly less compared with wild-type desmin filaments (500 ± 166 nm, $n = 54$; *t* test $p < 0.001$). Apparently, the observed structures represent short filament precursors. The desmin filaments formed by the p.R454W mutant did not differ significantly from wild-type desmin filaments in the *in vitro* assembly experiments (Fig. 4*F*).

Dual Color PALM Analysis of Filament Structure of ARVC-associated Desmin Mutants Co-expressed with Wild-type Desmin—Because all ARVC-associated desmin mutations presently known are heterozygous, we analyzed filament or aggregate formation in mutant and wild-type co-transfected cells. H9c2, C2C12, and HL-1 cells and hiPS-CM express endogenous cytoplasmic IF proteins. Therefore, we focused our analysis on transfected SW-13 cells, lacking endogenous cytoplasmic IF proteins (30), to characterize filament formation in a controlled heterozygous constellation.

To this end, we investigated whether wild-type and mutant desmin molecules co-exist in the same IF and whether filament assembly was disrupted by mutant desmin. Mutant and wild-type desmin were fused either with a thermostable variant of the green to red convertible fluorescent protein mEosFP termed mEosFP*thermo* (31–33) or with the green photoswitchable mIrisGFP1, a variant of IrisFP (24, 34, 35). After co-transfection with desmin expression constructs under the same constitutive promoter, filament formation was ana-

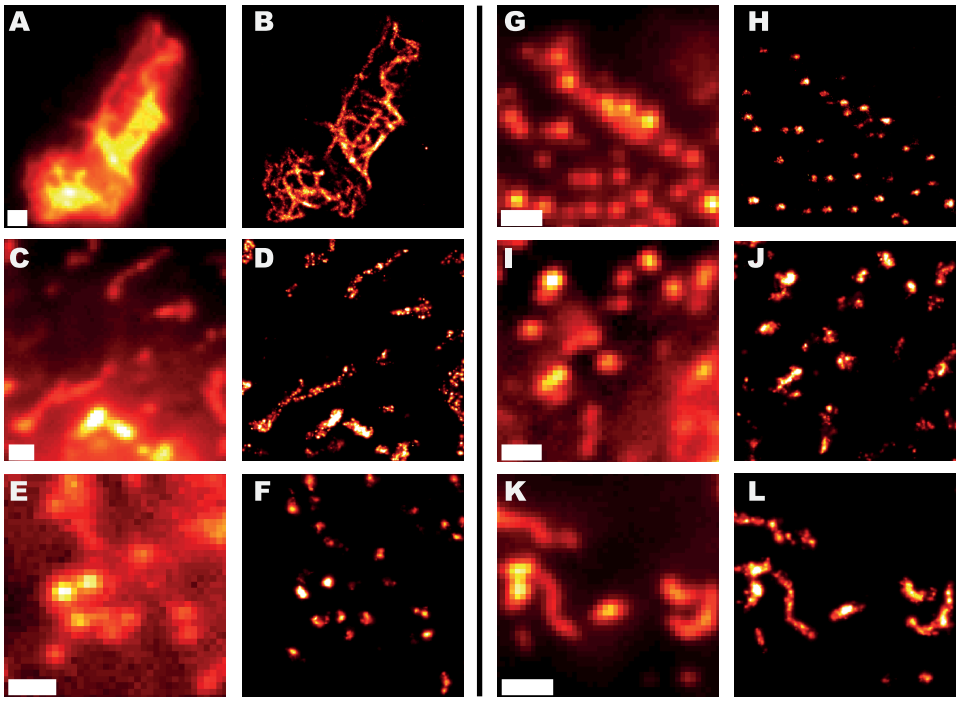

FIGURE 3. **PALM images of desmin mutation-expressing cells.** Representative wide field (*A*, *C*, *E*, *G*, *I*, and *K*) and the corresponding PALM images (*B*, *D*, *F*, *H*, *J*, and *L*) of desmin-mEosFP*thermo* transfected SW-13 cells are shown. *A* and *B*, wild type; *C* and *D*, p.S13F; *E* and *F*, p. E114del; *G* and *H*, p.N116S; *I* and *J*, p.N342D; *K* and *L*, p.R454W. The *scale bars* represent 1 μm.

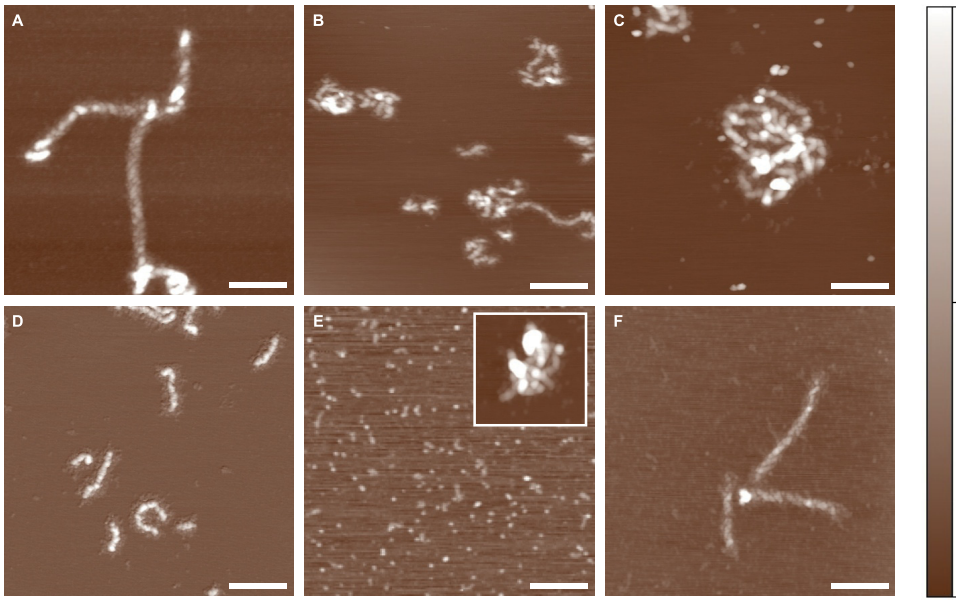

FIGURE 4. **Filament assembly of recombinant mutant desmin.** Desmin molecules were expressed in *E. coli* and purified by ion exchange and affinity chromatography. Filament assembly was initiated by the addition of sodium chloride. Representative AFM topography images are shown. *A*, wild type; *B*, p.S13F; *C*, p.N116S; *D*, p.E114del; *E*, p.N342D; *F*, p.R454W. Of note, the filament length of p.E114del (114 ± 55 nm, $n = 88$) is significantly lower (unpaired *t* test, $p < 0.001$) compared with wild-type filaments (500 ± 166 nm, $n = 54$; means ± S.D.). The height is color-coded. The *color scale bar* corresponds to a range of 5 nm (*A* and *F*), 10 nm (*B* and *C*), 7 nm (*D*), 2 nm (*E*), and 10 nm (*E*, *inset*). The *lateral scale bars* represent 200 nm (including *E*, *inset*).

lyzed in living cells by dual color PALM. This technique provides a roughly 10-fold improvement in resolution over conventional wide field microscopy (compare Fig. 3) (24, 25, 36).

As a result, co-expression of p.S13F (Fig. 5, *D–F*) or p.N116S (Fig. 5, *J–L*) with wild-type desmin led to filaments as well as aggregates in the same cell. In contrast, the co-expression of p.E114del in combination with wild-type desmin blocked filament formation completely because only cytoplasmic aggregates could be detected in transfected cells (Fig. 5, *G–I*). The co-expression of p.N342D (Fig. 5, *M–O*) or p.R454W (Fig. 5, *P–R*) with wild-type desmin led to an incorporation of mutant molecules into IF without aggregates similar to the controls (Fig. 5, *A–C*).

FRET Imaging of Co-expressed Mutant and Wild-type Desmin—To confirm the results of the PALM experiments with a second approach providing nearly molecular resolution on filament formation mimicking a heterozygous genotype, we

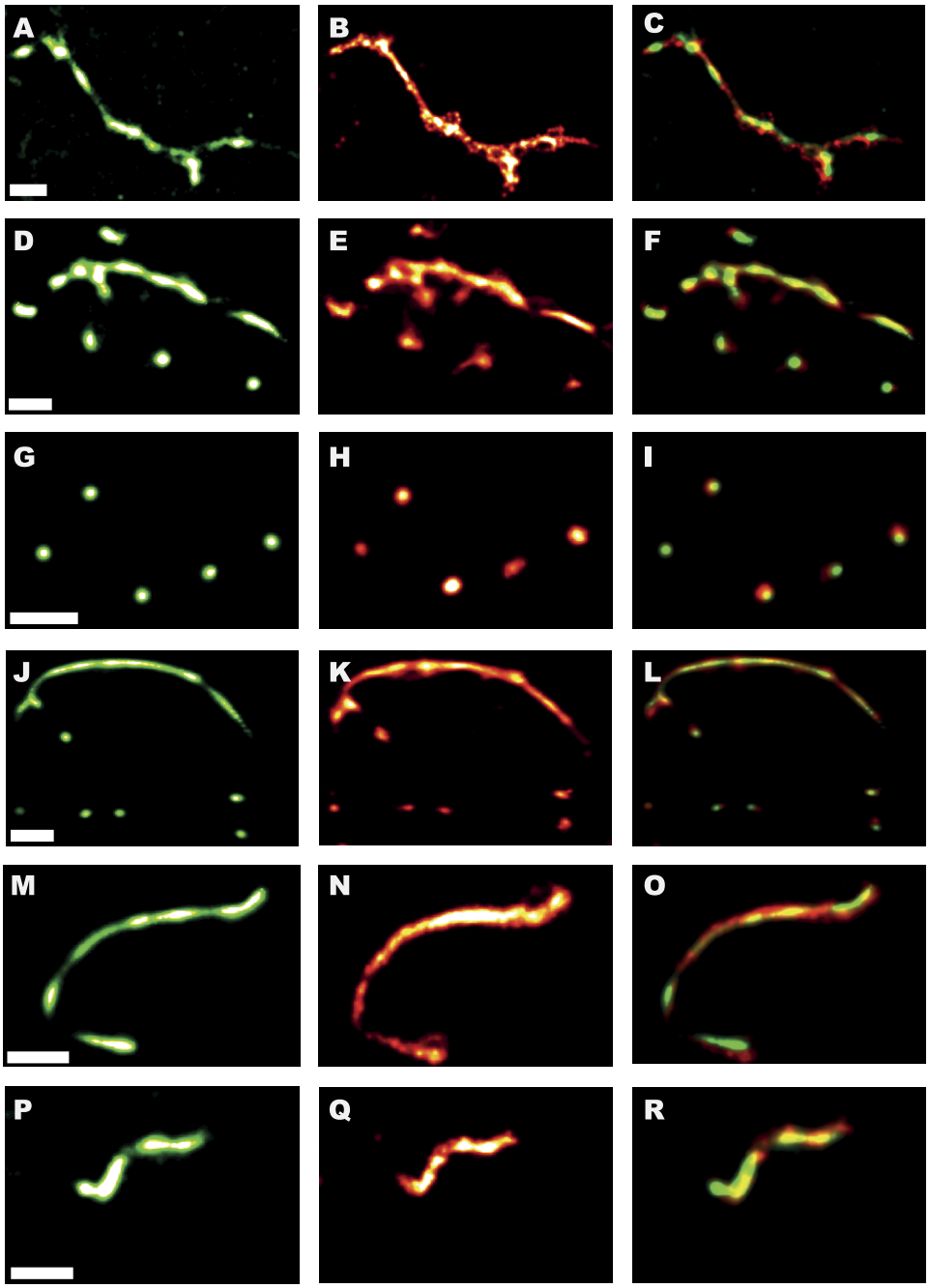

FIGURE 5. **Dual color PALM images of co-transfected cells.** Representative dual color PALM images of doubly transfected SW-13 cells are shown. Wild-type desmin was labeled with mIrisGFP1, and the mutant forms were labeled with mEosFP*thermo*. *A–C*, wild type; *D–F*, p.S13F; *G–I*, p.E114del; *J–L*, p.N116S; *M–O*, p.N342D; *P–R*, p.R454W. The images in the *left column* were detected in the green channel, and the images in the *middle column* were detected in the red channel, respectively. The *right column* shows overlays of both color channels. The *scale bars* represent 1 μm.

performed FRET microscopy by transfecting cells with enhanced cyan fluorescent protein- and eYFP-tagged desmins. FRET experiments provide additional information on the molecular assembly of desmin filaments and aggregates, because a strong FRET efficiency signal can only be detected if two proteins are in close proximity. We first performed a control experiment in filamentous structures with wild-type desmin fused to both fluorescence tags. We detected a FRET signal in all filaments (Fig. 6*A*), which indicates a suitable interprotein distance for this approach. We found that mutant desmin molecules p.S13F (Fig. 6*B*), p.N342D (Fig. 6*E*), and p.R454W (Fig. 6*F*) were incorporated together with wild-type desmin into the same filaments. No aggregates were detected in these co-transfected cells. In cells co-expressing p.N116S mutant and wild-type desmin, we observed a FRET signal in both small filaments as well as aggregates (Fig. 6*C*). In cells co-expressing the desmin mutant p.E114del in combination with the wild-type desmin FRET signal could be detected only in cytoplasmic aggregates (Fig. 6*D*), further revealing severe impairment of desmin fiber formation in this constellation. We conclude that mutant and wild-type desmin were co-assembled in both structures and that mutant desmin partially (p.N116S)

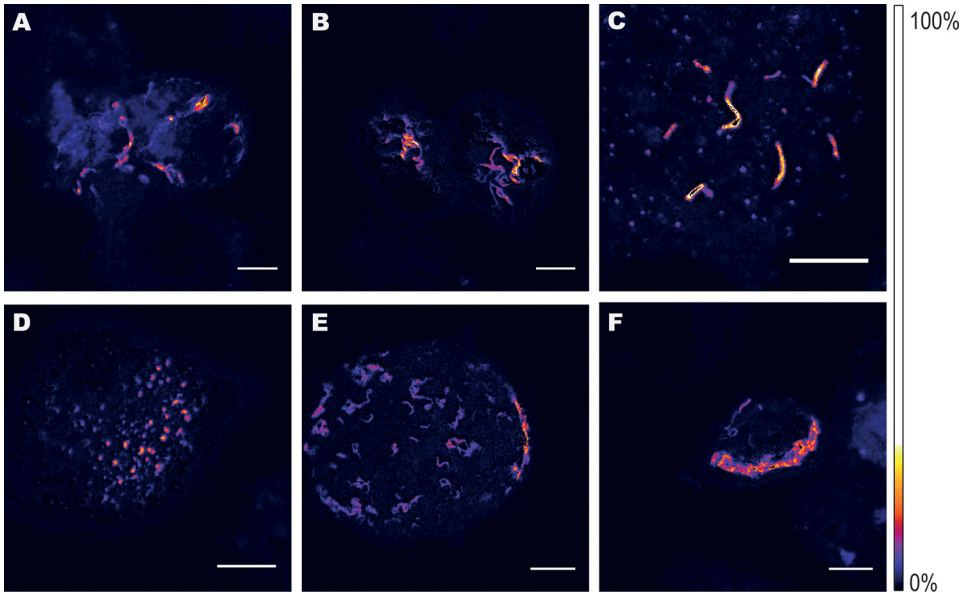

FIGURE 6. **FRET experiments of co-transfected cells.** Representative fluorescence images color-coded for FRET (0–100%) of SW-13 cells co-expressing wild-type and mutant desmin are shown. The wild-type desmin was labeled with eYFP, which acts as FRET acceptor, and the indicated mutant desmin molecules are labeled with enhanced cyan fluorescent protein, which acts as a FRET donor. *A*, wild type; *B*, p.S13F; *C*, p.N116S; *D*, p.E114del; *E*, p.N342D; *F*, p.R454W. The *scale bars* represent 5 μm.

or completely (p.E114del) prevents formation of functional filaments by wild-type desmin.

DISCUSSION

Up to now, more than 50 disease-causing *DES* mutations distributed over the entire amino acid sequence were identified (4). The disease phenotypes of these mutations are clinically heterogeneous, ranging from isolated myopathy, dilated cardiomyopathy with or without skeletal muscle disorder, and hypertrophic, restrictive, or arrhythmogenic right ventricular cardiomyopathy (37).

In this study, we have systematically compared the effects of five recently identified ARVC-associated *DES* mutations on filament formation to obtain further molecular insights into the assembly defects of this subgroup of mutants. We analyzed desmin filament formation in five different cell types ranging from human adenocarcinoma cells (SW-13) to human cardiomyocytes derived from hiPS to exclude putative influences of the cell environment on filament assembly defects. As a result, we did not find differences between the cell types used for the homozygous transfection. However, in these cell lines it was only possible to differentiate between desmin aggregates or filament formation, respectively (Fig. 7). Moreover, the *DES* mutations analyzed in our study are found in patients as a heterozygous genotype. Thus, this cell system is not directly comparable with the *in vivo* situation.

To analyze whether mutant desmin molecules are incorporated into common filaments of the wild-type form, we co-transfected SW-13 cells with mutant and wild-type desmin fused to different photoconvertible fluorescent proteins to be able to perform PALM imaging (38). As an additional approach, we analyzed filament formation in the same cell system by application of FRET.

We hypothesized that the heterozygous desmin genotype will result in remarkably different forms of desmin filament and

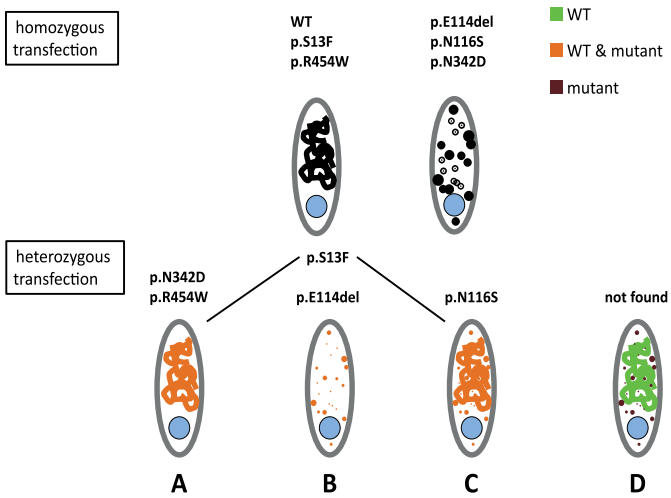

FIGURE 7. **Model depicting filament and/or aggregate formation of desmin mutants.**

aggregate formation compared with the homozygous cell culture model, because filament formation might be influenced by co-expression of mutant desmin according to the following types (compare Fig. 7): type A, only filaments are formed: mutant and wild-type molecules are incorporated within the same filament; type B, only aggregates are formed composed of a mixture of wild-type *and* mutant molecules; Type C, aggregates *and* filaments are found within the same cell: the aggregates and filaments are formed by mutant *and* wild-type desmin; and type D, aggregates *and* filaments are found within the same cell: wild-type desmin is found in filaments, whereas the mutant forms aggregates. To identify which of these types might be found in desminopathies, we analyzed cardiomyopathy-associated mutations in cell culture.

Sharma *et al.* (17) and Pica *et al.* (41) found equivocal results on the desmin mutant p.S13F, because it formed small fila-

ments and aggregates after homozygous transfection in different cell lines. In our experiments, the homozygous transfection of p.S13F reveals exclusively filaments in the majority of cells, whereas in the heterozygously transfected cells, we found mixed filaments of mutant and wild type, as well as cells with mixed filaments and aggregates. Thus, p.S13F forms filaments according to types A and C, respectively (Fig. 7). Serine 13 is localized within the conserved nonapeptide in the head domain, which is essential for filament assembly (39). The heterogeneous *in vitro* effects found with the mutant p.S13F might therefore be due to the degree of phosphorylation at serine 13 (40). It is remarkable that the ambiguous classification of the *in vitro* findings are paralleled by the heterogeneous clinical phenotype ranging from isolated myopathy to different forms of cardiomyopathy even within the same family (6, 7, 17, 41).

The mutant p.E114del revealed a severe filament formation defect *in vitro*, because we found exclusively cells with aggregates, which is consistent with previous studies on homozygously transfected SW-13, 3T3, and C2C12 cells (9). In the heterozygously transfected cells, mutant p.E114del showed a dominant effect even on wild-type desmin and led to aggregates, which also incorporated wild-type desmin according to type B (Fig. 7). This deletion mutant also impairs protein interactions with the IF protein synemin, resulting in a complete co-aggregation of both proteins (42). p.E114del presumably induces a twist of the hydrophobic seam, which is essential for formation of the coiled-coil dimer (9). We therefore conclude from our data that this mutant provides a dominant loss of the ability of wild-type desmin molecules to form filaments. Furthermore, the AFM experiments revealed that the longitudinal extension step is presumably impaired similar to the previously characterized mutations p.L385P and p.R406W (43), because this mutant forms significantly shorter filaments compared with the wild type.

Previously, we showed that the mutant p.N116S leads to aggregate formation when homozygously expressed in SW-13 cells. However, in the cardiac tissue of the patient, both filaments *and* aggregates of desmin were detectable (8). In the heterozygous cell culture experiments, mutant p.N116S forms also filaments *and* aggregates within the same cell composed of both desmin forms according to type C (Fig. 7).

In our study, homozygous expression of p.N342D desmin led to a phenotype comparable with the one previously described (29). However, when extending these investigations to heterozygous co-expression, we exclude a dominant inhibiting effect on filament assembly, because mutant and wild-type desmin molecules were incorporated into the same filamentous structures without aggregate formation according to type A (Fig. 7).

Different groups investigated the homozygous expression of p.R454W desmin in different cell lines, leading to conflicting results concerning the degree of aggregate formation (28, 44). In our hands, homozygously transfected p.R454W desmin formed filament networks independently of the cell type investigated. These results were confirmed by high resolution fluorescence microscopy and AFM experiments with purified desmin. Interestingly, our AFM data revealed right-handed helical filaments of wild-type and p.R454W desmin (Fig. 4), which are also known from the IF protein vimentin (45). Furthermore, we found that the heterozygously expressed p.R454W desmin forms mixed filaments in transfected cells according to type A (Fig. 7). Co-expression experiments were also reported by Bär *et al.* (46) leading to similar results. However, in that study, co-localization of wild-type and mutant desmin could not be analyzed for technical reasons. The amount of dimers, tetramers, and oligomers of p.R454W in transfected cells was previously determined by single particle fluorescence spectroscopy, demonstrating that p.R454W differs only marginally from the wild type (28). Consequently, the pathogenic role of this variant is not clear. Further studies might clarify the clinical impact of this sequence variant.

Our data clearly reveal that all of the mutants form mixed filaments or aggregates (Fig. 7, *types A–C*). Interestingly, in any of the mutations analyzed in this study, we did not observe a separation of mutant and wild-type desmin into filaments or aggregates within the same cell, respectively (Fig. 7, *type D*). Despite this systematic absence of segregation, it has to be noted that slight variations in the local concentration of mutant and wild-type desmin can be observed in the PALM images, as well as in the FRET images. Also, because of the sequential nature of the PALM image acquisition procedure, both color channels are affected by cell movement, resulting in a slight shift of the structures in the red and green channels, respectively. This is in agreement with previous reports describing IFs as dynamic structures that move in living cells (for a review see Ref. 47).

The detection of filaments composed of wild-type and mutant desmin raises the question of whether the nanomechanical properties of mixed filaments are impaired by the incorporation of the mutant forms. However, currently we cannot exclude that some other desmin mutants might lead to a type D filament formation defect.

The methodological approach of our study includes two complementary techniques for the analysis of desmin filament formation in living cells. Whereas the dual color PALM experiments provide insight into the structural composition of mutant and wild-type desmin, the FRET data reflect molecular interactions of these IF forms within the range below 10 nm. Because of the dual color PALM experiments, we could exclude for the investigated mutants the hypothetical type D filament formation defect, which is not detectable by FRET analysis.

In summary, our methodological approach using high resolution dual color PALM and FRET measurements substantially improves the understanding of the structures and the molecular assembly of heterozygously expressed mutants in living cells. In addition, the experiments led to a more sophisticated scheme of filament formation defects caused by *DES* mutations.

Acknowledgments—We thank James Thomson (University of Wisconsin, Madison, WI) for providing hiPS cells, Christine Mummery (Leiden University Medical Centre, Leiden, The Netherlands) for END2 cells, William Claycomb (New Orleans, LA) for providing HL-1 cells, and Désirée Gerdes, Birte Bohms, and Ramona Cebulla for excellent technical assistance. We thank Tim Skrzipczyk for support in cloning some plasmids and Florian Gärtner, Bernd Stratmann, Ines Stork, Doris Hendig, and Christoph Brodehl for helpful discussions.

REFERENCES

1. Goldfarb, L. G., Park, K. Y., Cervenáková, L., Gorokhova, S., Lee, H. S., Vasconcelos, O., Nagle, J. W., Semino-Mora, C., Sivakumar, K., and Dalakas, M. C. (1998) Missense mutations in desmin associated with familial cardiac and skeletal myopathy. *Nat. Genet.* **19,** 402–403
2. Goldfarb, L. G., and Dalakas, M. C. (2009) Tragedy in a heartbeat. Malfunctioning desmin causes skeletal and cardiac muscle disease. *J. Clin. Invest.* **119,** 1806–1813
3. Muñoz-Mármol, A. M., Strasser, G., Isamat, M., Coulombe, P. A., Yang, Y., Roca, X., Vela, E., Mate, J. L., Coll, J., Fernández-Figueras, M. T., Navas-Palacios, J. J., Ariza, A., and Fuchs, E. (1998) A dysfunctional desmin mutation in a patient with severe generalized myopathy. *Proc. Natl. Acad. Sci. U.S.A.* **95,** 11312–11317
4. Hong, D., Wang, Z., Zhang, W., Xi, J., Lu, J., Luan, X., and Yuan, Y. (2011) A series of Chinese patients with desminopathy associated with six novel and one reported mutations in the desmin gene. *Neuropathol Appl. Neurobiol.* **37,** 257–270
5. Bär, H., Strelkov, S. V., Sjöberg, G., Aebi, U., and Herrmann, H. (2004) The biology of desmin filaments. How do mutations affect their structure, assembly, and organisation? *J. Struct. Biol.* **148,** 137–152
6. van Tintelen, J. P., Van Gelder, I. C., Asimaki, A., Suurmeijer, A. J., Wiesfeld, A. C., Jongbloed, J. D., van den Wijngaard, A., Kuks, J. B., van Spaendonck-Zwarts, K. Y., Notermans, N., Boven, L., van den Heuvel, F., Veenstra-Knol, H. E., Saffitz, J. E., Hofstra, R. M., and van den Berg, M. P. (2009) Severe cardiac phenotype with right ventricular predominance in a large cohort of patients with a single missense mutation in the DES gene. *Heart Rhythm* **6,** 1574–1583
7. Otten, E., Asimaki, A., Maass, A., van Langen, I. M., van der Wal, A., de Jonge, N., van den Berg, M. P., Saffitz, J. E., Wilde, A. A., Jongbloed, J. D., and van Tintelen, J. P. (2010) Desmin mutations as a cause of right ventricular heart failure affect the intercalated disks. *Heart Rhythm* **7,** 1058–1064
8. Klauke, B., Kossmann, S., Gaertner, A., Brand, K., Stork, I., Brodehl, A., Dieding, M., Walhorn, V., Anselmetti, D., Gerdes, D., Bohms, B., Schulz, U., Zu Knyphausen, E., Vorgerd, M., Gummert, J., and Milting, H. (2010) *De novo* desmin-mutation N116S is associated with arrhythmogenic right ventricular cardiomyopathy. *Hum. Mol. Genet* **19,** 4595–4607
9. Vernengo, L., Chourbagi, O., Panuncio, A., Lilienbaum, A., Batonnet-Pichon, S., Bruston, F., Rodrigues-Lima, F., Mesa, R., Pizzarossa, C., Demay, L., Richard, P., Vicart, P., and Rodriguez, M. M. (2010) Desmin myopathy with severe cardiomyopathy in a Uruguayan family due to a codon deletion in a new location within the desmin 1A rod domain. *Neuromuscul. Disord.* **20,** 178–187
10. Kartenbeck, J., Franke, W. W., Moser, J. G., and Stoffels, U. (1983) Specific attachment of desmin filaments to desmosomal plaques in cardiac myocytes. *EMBO J.* **2,** 735–742
11. Capetanaki, Y., Bloch, R. J., Kouloumenta, A., Mavroidis, M., and Psarras, S. (2007) Muscle intermediate filaments and their links to membranes and membranous organelles. *Exp. Cell Res.* **313,** 2063–2076
12. Herrmann, H., and Aebi, U. (2004) Intermediate filaments. Molecular structure, assembly mechanism, and integration into functionally distinct intracellular Scaffolds. *Annu. Rev. Biochem.* **73,** 749–789
13. Nicolet, S., Herrmann, H., Aebi, U., and Strelkov, S. V. (2010) Atomic structure of vimentin coil 2. *J. Struct. Biol.* **170,** 369–376
14. Chernyatina, A. A., Nicolet, S., and Strelkov, S. V. (2011) 7th European Conference on Intermediate Filaments in Health and Disease, Mykonos, Greece, June 16–19, 2011 (Capetanaki, Y., and Mavroidis, M., eds) European Society for Intermediate Filament Biology
15. Herrmann, H., Strelkov, S. V., Burkhard, P., and Aebi, U. (2009) Intermediate filaments. Primary determinants of cell architecture and plasticity. *J. Clin. Invest.* **119,** 1772–1783
16. Bar, H., Fischer, D., Goudeau, B., Kley, R. A., Clemen, C. S., Vicart, P., Herrmann, H., Vorgerd, M., and Schroder, R. (2005) Pathogenic effects of a novel heterozygous R350P desmin mutation on the assembly of desmin intermediate filaments *in vivo* and *in vitro*. *Hum. Mol. Genet* **14,** 1251–1260
17. Sharma, S., Mücke, N., Katus, H. A., Herrmann, H., and Bär, H. (2009) Disease mutations in the "head" domain of the extra-sarcomeric protein desmin distinctly alter its assembly and network-forming properties. *J. Mol. Med.* **87,** 1207–1219
18. Claycomb, W. C., Lanson, N. A., Jr., Stallworth, B. S., Egeland, D. B., Delcarpio, J. B., Bahinski, A., and Izzo, N. J., Jr. (1998) HL-1 cells. A cardiac muscle cell line that contracts and retains phenotypic characteristics of the adult cardiomyocyte. *Proc. Natl. Acad. Sci. U.S.A.* **95,** 2979–2984
19. Yu, J., Vodyanik, M. A., Smuga-Otto, K., Antosiewicz-Bourget, J., Frane, J. L., Tian, S., Nie, J., Jonsdottir, G. A., Ruotti, V., Stewart, R., Slukvin, I. I., and Thomson, J. A. (2007) Induced pluripotent stem cell lines derived from human somatic cells. *Science* **318,** 1917–1920
20. Mummery, C., Ward-van Oostwaard, D., Doevendans, P., Spijker, R., van den Brink, S., Hassink, R., van der Heyden, M., Opthof, T., Pera, M., de la Riviere, A. B., Passier, R., and Tertoolen, L. (2003) Differentiation of human embryonic stem cells to cardiomyocytes. Role of coculture with visceral endoderm-like cells. *Circulation* **107,** 2733–2740
21. Gupta, M. K., Illich, D. J., Gaarz, A., Matzkies, M., Nguemo, F., Pfannkuche, K., Liang, H., Classen, S., Reppel, M., Schultze, J. L., Hescheler, J., and Sarić, T. (2010) Global transcriptional profiles of beating clusters derived from human induced pluripotent stem cells and embryonic stem cells are highly similar. *BMC Dev. Biol.* **10,** 98
22. Kreplak, L., Bär, H., Leterrier, J. F., Herrmann, H., and Aebi, U. (2005) Exploring the mechanical behavior of single intermediate filaments. *J. Mol. Biol.* **354,** 569–577
23. Hedde, P. N., Fuchs, J., Oswald, F., Wiedenmann, J., and Nienhaus, G. U. (2009) Online image analysis software for photoactivation localization microscopy. *Nat. Methods* **6,** 689–690
24. Fuchs, J., Böhme, S., Oswald, F., Hedde, P. N., Krause, M., Wiedenmann, J., and Nienhaus, G. U. (2010) A photoactivatable marker protein for pulse-chase imaging with superresolution. *Nat. Methods* **7,** 627–630
25. Shroff, H., Galbraith, C. G., Galbraith, J. A., White, H., Gillette, J., Olenych, S., Davidson, M. W., and Betzig, E. (2007) Dual-color superresolution imaging of genetically expressed probes within individual adhesion complexes. *Proc. Natl. Acad. Sci. U.S.A.* **104,** 20308–20313
26. Clegg, R. M. (1992) Fluorescence resonance energy transfer and nucleic acids. *Methods Enzymol.* **211,** 353–388
27. Hachet-Haas, M., Converset, N., Marchal, O., Matthes, H., Gioria, S., Galzi, J. L., and Lecat, S. (2006) FRET and colocalization analyzer. A method to validate measurements of sensitized emission FRET acquired by confocal microscopy and available as an ImageJ Plug-in. *Microsc. Res. Tech.* **69,** 941–956
28. Levin, J., Bulst, S., Thirion, C., Schmidt, F., Bötzel, K., Krause, S., Pertl, C., Kretzschmar, H., Walter, M. C., Giese, A., and Lochmüller, H. (2010) Divergent molecular effects of desmin mutations on protein assembly in myofibrillar myopathy. *J. Neuropathol. Exp. Neurol.* **69,** 415–424
29. Dalakas, M. C., Dagvadorj, A., Goudeau, B., Park, K. Y., Takeda, K., Simon-Casteras, M., Vasconcelos, O., Sambuughin, N., Shatunov, A., Nagle, J. W., Sivakumar, K., Vicart, P., and Goldfarb, L. G. (2003) Progressive skeletal myopathy, a phenotypic variant of desmin myopathy associated with desmin mutations. *Neuromuscul. Disord.* **13,** 252–258
30. Hedberg, K. K., and Chen, L. B. (1986) Absence of intermediate filaments in a human adrenal cortex carcinoma-derived cell line. *Exp. Cell Res.* **163,** 509–517
31. Nienhaus, K., Nienhaus, G. U., Wiedenmann, J., and Nar, H. (2005) Structural basis for photo-induced protein cleavage and green-to-red conversion of fluorescent protein EosFP. *Proc. Natl. Acad. Sci. U.S.A.* **102,** 9156–9159
32. Wiedenmann, J., Ivanchenko, S., Oswald, F., Schmitt, F., Röcker, C., Salih, A., Spindler, K. D., and Nienhaus, G. U. (2004) EosFP, a fluorescent marker protein with UV-inducible green-to-red fluorescence conversion. *Proc. Natl. Acad. Sci. U.S.A.* **101,** 15905–15910
33. Nienhaus, G. U., Nienhaus, K., Hölzle, A., Ivanchenko, S., Renzi, F., Oswald, F., Wolff, M., Schmitt, F., Röcker, C., Vallone, B., Weidemann, W., Heilker, R., Nar, H., and Wiedenmann, J. (2006) Photoconvertible fluorescent protein EosFP. Biophysical properties and cell biology applications. *Photochem. Photobiol.* **82,** 351–358
34. Adam, V., Lelimousin, M., Boehme, S., Desfonds, G., Nienhaus, K., Field, M. J., Wiedenmann, J., McSweeney, S., Nienhaus, G. U., and Bourgeois, D.

(2008) Structural characterization of IrisFP, an optical highlighter undergoing multiple photo-induced transformations. *Proc. Natl. Acad. Sci. U.S.A.* **105,** 18343–18348
35. Wiedenmann, J., Gayda, S., Adam, V., Oswald, F., Nienhaus, K., Bourgeois, D., and Nienhaus, G. U. (2011) From EosFP to mIrisFP. Structure-based development of advanced photoactivatable marker proteins of the GFP-family. *J. Biophotonics* **4,** 377–390
36. Andresen, M., Stiel, A. C., Fölling, J., Wenzel, D., Schönle, A., Egner, A., Eggeling, C., Hell, S. W., and Jakobs, S. (2008) Photoswitchable fluorescent proteins enable monochromatic multilabel imaging and dual color fluorescence nanoscopy. *Nat. Biotechnol.* **26,** 1035–1040
37. van Spaendonck-Zwarts, K., van Hessem, L., Jongbloed, J. D., de Walle, H. E., Capetanaki, Y., van der Kooi, A. J., van Langen, I. M., van den Berg, M. P., and van Tintelen, J. P. (2010) *Clin. Genet.* **89,** 354–366
38. Hedde, P. N., and Nienhaus, G. U. (2010) Optical imaging of nanoscale cellular structures. *Biophys. Rev.* **2,** 147–158
39. Raats, J. M., Pieper, F. R., Vree Egberts, W. T., Verrijp, K. N., Ramaekers, F. C., and Bloemendal, H. (1990) Assembly of amino-terminally deleted desmin in vimentin-free cells. *J. Cell Biol.* **111,** 1971–1985
40. Kitamura, S., Ando, S., Shibata, M., Tanabe, K., Sato, C., and Inagaki, M. (1989) Protein kinase C phosphorylation of desmin at four serine residues within the non-α-helical head domain. *J. Biol. Chem.* **264,** 5674–5678
41. Pica, E. C., Kathirvel, P., Pramono, Z. A., Lai, P. S., and Yee, W. C. (2008) Characterization of a novel S13F desmin mutation associated with desmin myopathy and heart block in a Chinese family. *Neuromuscul. Disord.* **18,** 178–182
42. Chourbagi, O., Bruston, F., Carinci, M., Xue, Z., Vicart, P., Paulin, D., and Agbulut, O. (2011) Desmin mutations in the terminal consensus motif prevent synemin-desmin heteropolymer filament assembly. *Exp. Cell Res.* **317,** 886–897
43. Bär, H., Mücke, N., Kostareva, A., Sjöberg, G., Aebi, U., and Herrmann, H. (2005) Severe muscle disease-causing desmin mutations interfere with *in vitro* filament assembly at distinct stages. *Proc. Natl. Acad. Sci. U.S.A.* **102,** 15099–15104
44. Bär, H., Goudeau, B., Wälde, S., Casteras-Simon, M., Mücke, N., Shatunov, A., Goldberg, Y. P., Clarke, C., Holton, J. L., Eymard, B., Katus, H. A., Fardeau, M., Goldfarb, L., Vicart, P., and Herrmann, H. (2007) Conspicuous involvement of desmin tail mutations in diverse cardiac and skeletal myopathies. *Hum. Mutat.* **28,** 374–386
45. Ando, S., Nakao, K., Gohara, R., Takasaki, Y., Suehiro, K., and Oishi, Y. (2004) Morphological analysis of glutaraldehyde-fixed vimentin intermediate filaments and assembly-intermediates by atomic force microscopy. *Biochim. Biophys. Acta* **1702,** 53–65
46. Bär, H., Schopferer, M., Sharma, S., Hochstein, B., Mücke, N., Herrmann, H., and Willenbacher, N. (2010) Mutations in desmin's carboxy-terminal "tail" domain severely modify filament and network mechanics. *J. Mol. Biol.* **397,** 1188–1198
47. Helfand, B. T., Chang, L., and Goldman, R. D. (2003) The dynamic and motile properties of intermediate filaments. *Annu. Rev. Cell Dev. Biol.* **19,** 445–467